Methods – Sampling, observations and at-sea analyses

WP BLM (Boundary Layer Meteorology)

O. Persson, B. Brooks, J. Prytherch, D. Wolfe, G. Sotiropoulou

The overriding goal of the Arctic Clouds in Summer Experiment (ACSE), also SWERUS WP I, is to better understand Arctic clouds and their role in regulating the surface energy balance. Another related objective is to understand how processes that modulate the surface energy balance are themselves affected by the transitions between open water and ice-covered areas in summer and early autumn. Clouds are known to have a profound influence on climate, reflecting solar radiation back to space and trapping infrared radiation near the surface. In the Arctic the surface energy balance is dominated by processes relating to low clouds, and hence these have an important impact on the freezing and melting of the sea ice. The structure and stability of the Arctic atmospheric boundary layer likely differs over sea ice compared to over open water, and this difference greatly impacts the various components of the surface energy budget, including those related to clouds.

Low clouds and fog are abundant in the Arctic, climatologically cover the surface 60-100% of the time, more in summer than in winter. In the summer Arctic where the sun is low but above the horizon most of the time, the effects of low clouds can vary greatly from over open-ocean to areas covered by sea ice because of the difference in surface albedo, and their effect is different from similar clouds over other world oceans. In short, while low clouds reflect solar radiation and hence limit the available energy at the surface, they absorb longwave radiation from the surface but also emit longwave radiation back to the surface, thus increasing the available energy at the surface. With a high surface albedo as over the sea ice, the longwave ("greenhouse") effect often dominates at all times except in the middle of summer, and the surface is heated by low clouds. In such areas and times, the surface temperature often falls when it becomes clear. Over the open ocean where the albedo is low, solar radiation dominates to an even greater extent during mid-summer, and its dominance persists longer into the autumn. These radiative effects also depend on and interact with the dynamics of the system, both the local cloud and boundary-layer dynamics and the larger-scale motions of the atmosphere which bring air of differing origins to a given location.

Low clouds that have a layer of liquid water are efficient at emitting longwave radiation, thus heating the surface but also cooling the cloud top. The latter destabilizes the vertical column of air and drives buoyant vertical motions – turbulence – that may mix to the surface depending on the stability of the lowest layers of the atmosphere known as the boundary layer. Furthermore, the downwelling longwave radiation depends on the temperature of these clouds, with warmer clouds enhancing the downwelling radiation. If the cloud top temperature is below zero, precipitation may form as ice crystals in the super cooled liquid layer, producing so called mixed-phase clouds. Such clouds are common in the Arctic but the interplay between thermal advection, radiation, turbulence, cloud microphysics and precipitation is poorly understood. Hence, the representation in models of the physics involved is inadequate, and hence weather and climate models struggle to get this right.

The large-scale atmospheric flow may bring warm and moist air from south or cold, dry and clean air from north. These new air masses are gradually brought into balance with the local surface, whether sea ice or open water, through energy fluxes. These energy fluxes likely differ significantly over melting sea ice (where the surface temperature is locked to near freezing), freezing sea ice with a varying surface temperature, and warmer open water. These advective processes also affect the properties of the clouds, and hence the surface energy balance.

The goal of ACSE is to understand these processes better, and to do so necessitates simultaneous measurements of the vertical structure of the atmosphere in general, cloud properties in particular and also the surface energy fluxes and characteristics. These measurements need to be carried out over the open water, near the marginal ice zone, and within the pack ice of the Arctic Ocean. During Leg 1, summer melting conditions were encountered on a fairly extensive pack ice area (Fig. BLM1), while during Leg 2 melting conditions were initially encountered (Fig. BLM2a) but some initial freeze-up conditions were also measured towards the end of this leg (Fig. BLM2b).

To make these measurements on a moving ship is a challenge. We accomplish this by making continuous observations through the whole expedition of the primary parameters, regardless of station or transit between stations, starting and ending in Tromsø, Norway, with an exchange of science crew in Barrow, Alaska (which also marked the transition between Leg 1 and Leg 2). Only the wave buoy measurements depended on stations. Though the cruise track was determined by the other SWERUS objectives, the track included extensive periods of open water and pack ice conditions, and numerous crossing of the Marginal Ice Zone (MIZ). Such mixed conditions allow the above objectives to be met.

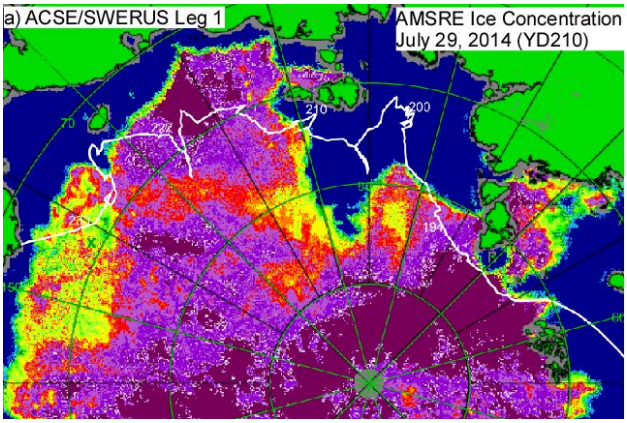

Fig. BLM1: The ACSE/SWERUS track for Leg 1. The Year Day is at times shown on the track corresponding to the Oden location on that day.

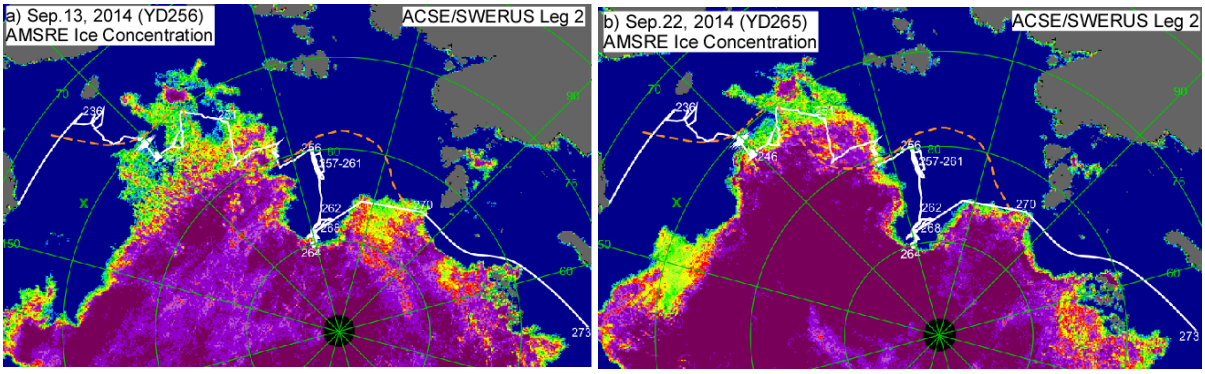

Fig. BLM2: The ACSE/SWERUS track for Leg 2 showing sea-ice concentrations on a) Sep 13, the approximate minimum sea ice extent, and b) Sep 26. The Sep 26 ice concentration shows an increase within the exisiting ice areas and an increase in extent in some regions (e.g., the Beaufort Sea). The Year Day is at times shown on the track corresponding to the Oden location on that day. The approximate location of the Russian Exclusive Economic Zone is shown as a brown dashed line.

Three main types of instrumentation systems were used and are described below, as are the involved technology and methods.

Equipment

General meteorology observations

The general meteorology observations provide context to the more specialized observations described below. This program has two main components (total amount of data is 4GB for the weather station and 5GB for the soundings):

1) Weather station: This consists of a combination of instruments located on and in front of the railing in the forward center of the 7th deck of Oden, logged on a common logger all sampled at 1Hz:
   a. Wind speed and direction with a Gill 2D Ultrasonic anemometer
   b. Position and horizontal motions with a Garmin GPS
   c. Temperature and relative humidity with a platinum resistor thermometer and a capacitive hygrometer, respectively
   d. Local atmospheric pressure with an electronic barometer.
   e. Incoming short and longwave radiation are measured with Eppley pyrano- and pyrgeometers, respectively, mounted on a gimbaled platform. The gimbal for the pyranometer (pyrgeometer) was immobilized at 01:40 UTC (01:50 UTC) on Sep. 2 because relative winds from the bow of 6-9 m/s or more caused a tilt of up to 15-20 degrees.
   f. Additional to this, but logged separately at one minute intervals and sampled as one minute averages, are a visibility sensor and a cloud base lidar (so called ceilometer). Both are based on lidar technology.

   All these instruments, with the exception of the GPS system and the ultrasonic anemometer, are from Vaisala Oy.

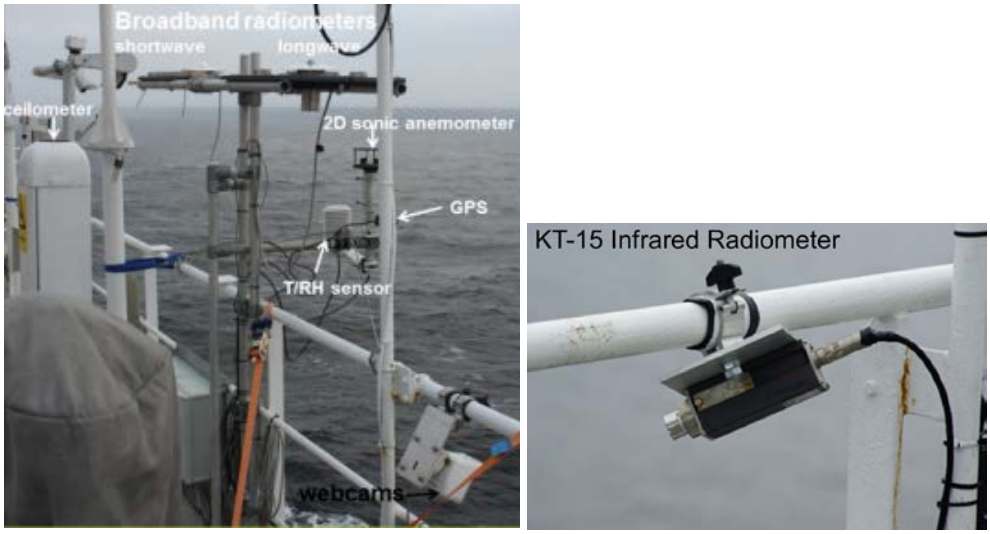

Fig. BLM3: Meteorological instruments deployed on the 7th deck of the Oden and discussed in the text.

2) Rawinsondes: Soundings through the entire troposphere and into the stratosphere are performed with free-flying helium-filled balloons carrying Vaisala RSG92 rawinsondes (sonde); soundings are released every 6 hours from the helideck of Oden (Fig. BLM4). The receiving station for the system is located on the 7th deck, in the port side container. Each sonde carries a barometer, thermometer and a hygrometer providing profiles of the state of the atmosphere; the techniques

used are similar to instruments on the weather station but less expensive since they are expendable. Additionally, a GPS sensor on the sonde measures the track of the sonde; this is the same as the wind, so the sonde also provide profiles of wind speed and direction.

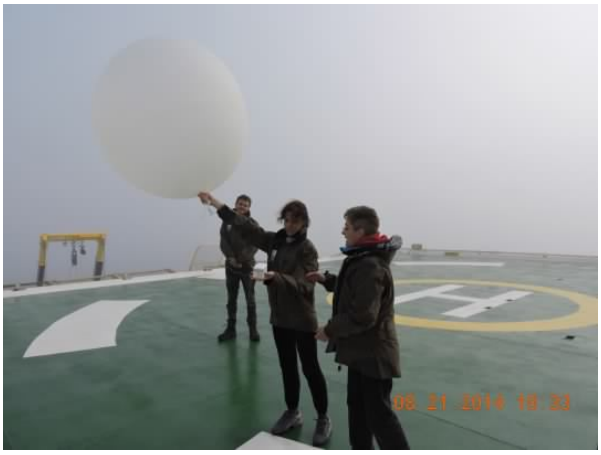

Fig. BLM4: Launch of a rawinsonde weather balloon during Leg 2.

Surface flux observations

Near surface atmospheric turbulence and the associated turbulent exchange of momentum, heat, water vapor and aerosol particles were made through the cruise, using so-called eddy-covariance technique. The system consists of several instruments installed at the top of the foremast.

1) At the top of the mast (total amount of data for leg 2 is 70GB):
   a. One heated Metek sonic anemometer (BLM5a) measures the 3-dimensional turbulent velocity of the air flow at 20Hz. Along with this an XSens MTi-G-700 inertial motion unit that provides 3D accelerations, rotation rates, and GPS position at 40Hz. The frame of reference is aligned with that of the sonic anemometer. The measurements are combined with those from the ship's navigation system (heading, speed and course over ground) to correct the turbulent wind measurements for ship motion. An example of partially processed data is given in Fig. BLM6.
   b. One Licor LI-7500 open path gas analyzer – water vapor concentration also at 20Hz (Fig. BLM5a); when combined with the vertical velocities from the Metek it provides turbulence fluxes of water vapor.
   c. One CLASP aerosol spectrometer sampled at 10Hz. This provides particle size spectra for the size range $0.25 < R < 18.5\mu m$, with 16 logarithmically spaced size bins.
   d. Temperature and relative humidity sampled at 1Hz from instruments mounted in a fan-aspirated and radiation protected shield.
2) One third down the mast (Leg 2 data amount est. 18 GB):
   a. One CSAT-3 sonic anemometer (Fig. BLM5b) mounted on a 1.5 m boom directed forward measures the 3-dimensional turbulent velocity of the air flow at 20Hz. On the same boom as the CSAT, an XSens MTi-G-700 inertial motion unit provides 3D accelerations, rotation rates, and GPS position at 40Hz. This will be used to process the sonic data.
   b. Temperature and relative humidity sampled at 1Hz from instruments mounted in a fan-aspirated and radiation protected shield.
   c. In addition to this flux system we sampled the high-rate data from Patrick Crill's LGR mass spectrometer system on the mast platform, drawing its sample from the top of the mast. This will enable turbulent fluxes of methane and carbon dioxide to be estimated.

Figure BLM5: Photos of the turbulence/surface flux instruments with (left) the top Metek/Licor/CLASP instrumentation with its motion sensor, and (right) the CSAT sonic on its retractable boom with the motion sensor mounted.

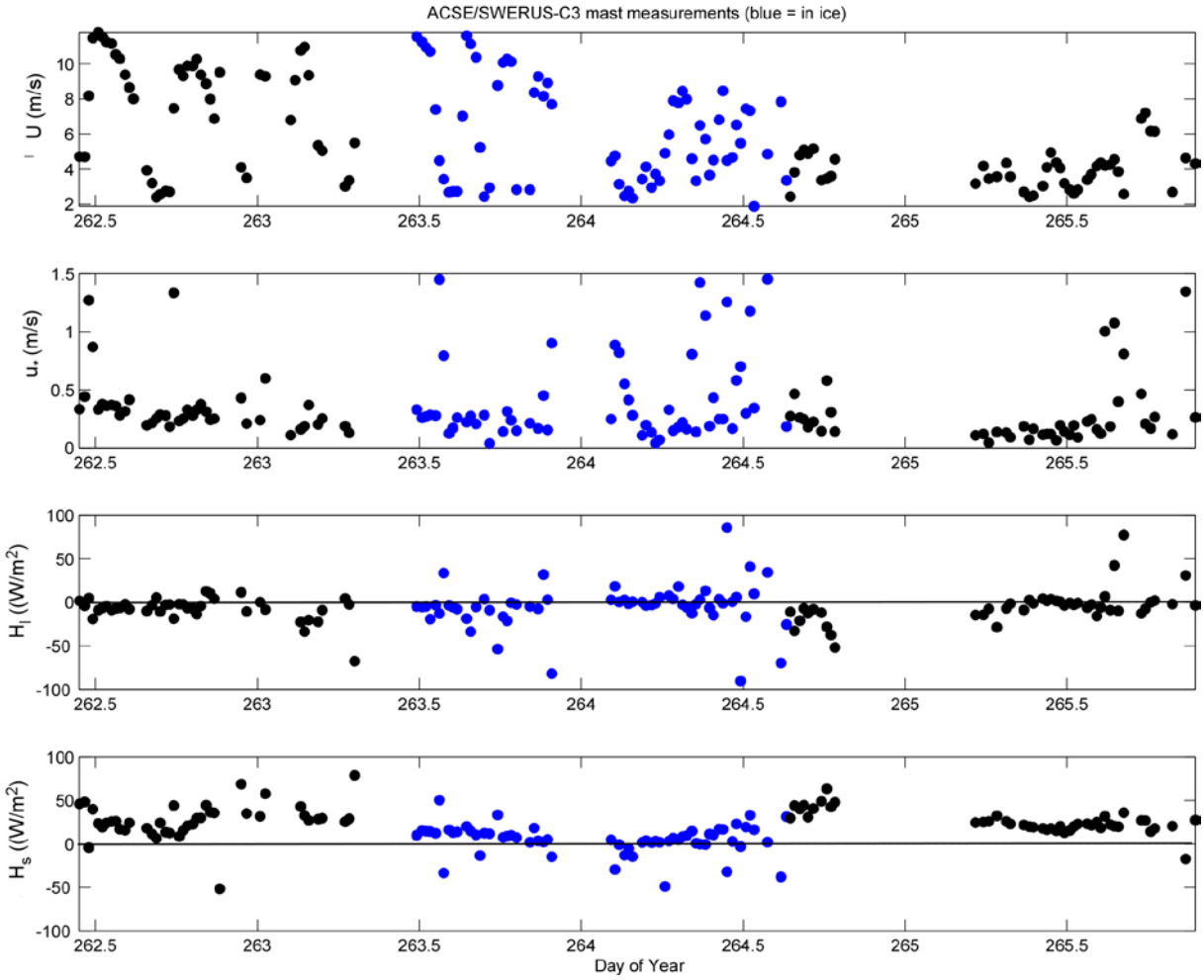

Figure BLM6: Plots of very preliminary (a) wind speed, b) friction velocity (momentum flux), c) latent heat flux, and d) sensible heat flux from the Metek sonic anemometer using eddy covariance techniques for Sep 19-22 (YD262-265). Ship distortion corrections have not been applied, but correction for ship motion has been. Blue (black) points are in ice (open water).

Surface based remote sensing

Surface based remote sensing relies on either active instruments (radar or lidar) or passive instruments (microwave radiometers). The former transmit energy and senses both the strength of the returned signal and its Doppler shift, while the latter senses naturally emitted radiation from the atmosphere at different wavelength, emitted by different atmospheric constituents according to their temperature. We have deployed several such instruments.

1) W-band Cloud Radar**:** This is a NOAA-built cloud radar that was operated from the sea container in position 11 on the roof of Oden's foredeck lab (Fig. BLM7a). The system operates at 94-GHz and nominally points vertically. It is operated on a motion stabilizing platform designed to maintain the radar level in spite of ship's pitch and roll motions. Measurements include profiles of the full Doppler spectrum that results from backscatter of transmitted signals from hydrometeors in the vertical column. From the spectrum, standard radar moments are derived, including the reflectivity, mean Doppler velocity, and Doppler spectrum width. The system has operated near-continuously for the duration of Leg 2. Many files are produced each day including hourly raw Doppler spectra, Doppler moments, instrument health messages, and output from the positioning system for the motion stabilized platform. Total data volume for Leg #2 is: 60 GB (moments); 900 GB (spectra); 9 GB (logs).

2) 449-MHz Wind Profiler**.** The wind profiler design was originally built at NOAA and is a phased-array Doppler radar operating with 5 fixed beams. The antenna is mounted above the containers placed on top of Oden's main lab (Fig. BLM7a). It has two operational modes with vertical resolutions of 62 m and 400 m. Transmitted pulses reflect off of radial gradients in the atmospheric refractive index. Using Fourier transform techniques, the system converts raw reflected signals into averaged Doppler spectra that are then analyzed to produce information about the radial velocities and backscatter magnitude. These data are used to estimate hourly profiles of wind speed and direction. The 449 MHz radar operates continuously, and has been very reliable during the cruise but continues to have issues with so-called ground clutter; effects on the so-called side lobes of the instrument by the ocean surface especially as it passes by when the ship is moving. The system produces two daily raw files and two daily, first-estimate wind profile files. Total data volume for Leg 2: 46 GB.

3) LIDAR: A Halo Photonics scanning Doppler lidar was installed on the roof of the CTD winch container (Fig. BLM7a). The lidar measures the intensity of backscatter laser light, providing a measure of atmospheric particle loading and along-beam Doppler wind speed. Cross-polarization provides additional information on particle shape allowing cloud droplets and ice crystals to be distinguished. The lidar operated in multiple scan modes. Most of its time is spent staring vertically upwards to measure boundary layer structure and cloud. Every 10 minutes a 5-point wind profile is measured (vertical + 4 off-vertical (70° elevation) beams at azimuths of 0,90,180,270 allow a single wind profile to be estimated), every hour 0-90° elevation scans were undertaken forward over the bow and 30° either side, along with a single horizontal scan at an elevation of 0°. To keep the lidar pointing in the correct attitude it was mounted within a motion stabilized platform that keeps it within about 0.1° of the horizontal most of the time. The residual linear velocity of the platform (heave and ship horizontal motion) is monitored and can be used to correct the lidar Doppler velocity for ship motion. Data volume is approximately 1GB per day (processed output) + 19GB per day (raw binary data files) (840 GB for Leg 2). The lidar data will be used to provide boundary layer wind profiles, information on vertical structure and mixing, turbulence intensity throughout the depth of the boundary layer, and information on cloud phase.

4) HATPRO Scanning Microwave Radiometer: The HATPRO scanning radiometer mounted on the roof of the 4th deck triple-container lab makes a scan from 0-90° elevation over the bow, measuring the microwave brightness temperature at multiple wavelengths. Given an initial best guess of the vertical profile of temperature and humidity, high temporal resolution (5 minute) profiles of temperature and humidity, along with integrated precipitable water vapor and liquid water path can be retrieved. During the cruise the initial best guess profile is provided by a climatological profile for the Arctic. In post processing the radiosonde profiles will be used. Cruise retrievals are available immediately while reprocessed data will be available in approximately 6 months. Approximate data volume: 123MB per day, 5.7GB total.

5) Radiometrics Scanning Microwave Radiometer (MWR)**:** A scanning Radiometrics MP-3000 multi-channel microwave radiometer was installed on the corner block of the CTD winch container in position 10 on Oden. It measures downwelling sky brightness temperatures in the range of 20-30 GHz, to derive the integrated liquid water and water vapor in the atmosphere (e.g., see Fig. BLM11b), and in the range of 50-60GHz, to derive profiles of atmospheric temperature and moisture. First-estimate geophysical parameters are derived operationally with a default retrieval algorithm that has been applied during the cruise. Best-estimate geophysical parameters will be

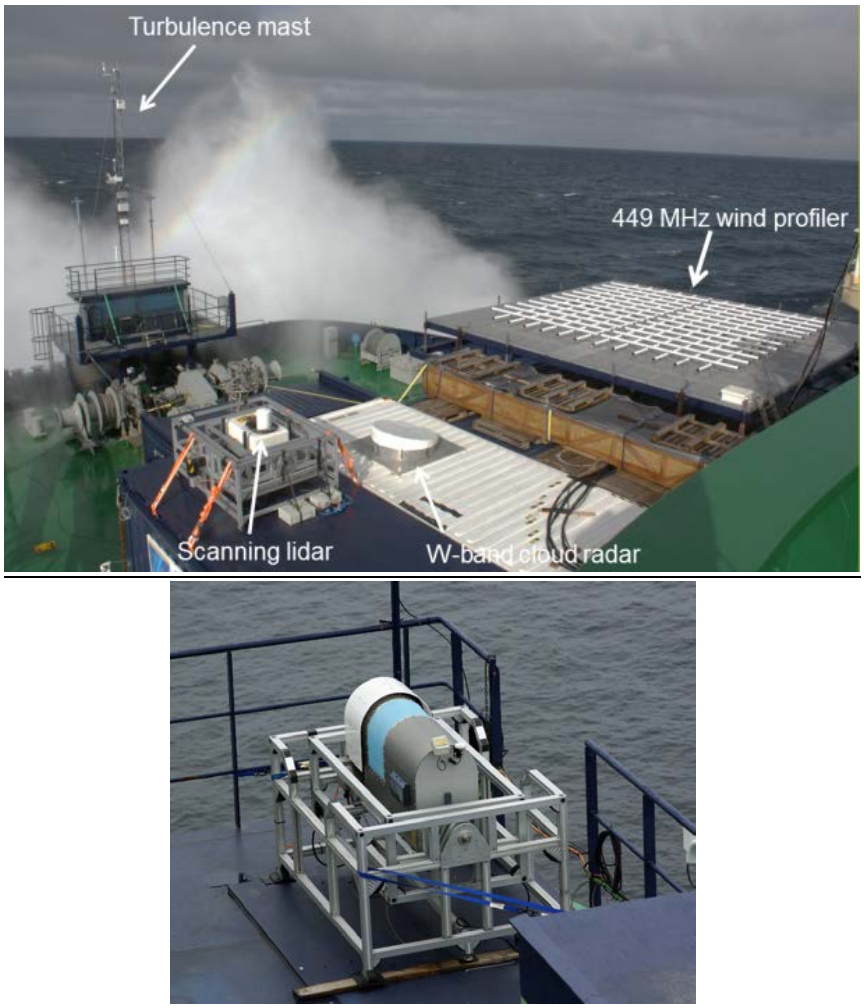

Figure BLM7: Photo of remote sensing instruments on Oden's foredeck (top) and the HATPRO scanning radiometer (bottom). Hidden from view are the MWR radiometer, on same container as the lidar, and the ceilometer behind the radar container. The turbulence mast is also shown.

derived post facto using input from rawinsonde measurements of temperature and moisture structure during the cruise itself. Operations during leg #2 of the cruise have been fairly clean with minimal interruption. Data are provided in a suite of 5 ASCII files (lv0, lv1, lv2, tip, ser), all containing header information that describes the fields, measurement units, operational modes, etc. "ser" files are instrument logs, "tip" files contain calibration information, "lv0" files contain raw voltage measurements, "lv1" files contain brightness temperature measurements, and "lv2" files contain the first-estimated retrievals of geophysical parameters. Total data volume for leg 2: 750 MB.

6) Ceilometer: A Vaisala CT-31 ceilometer was installed to the rear of the sea container in position 11. It uses a near-infrared laser to derive the atmospheric backscatter and specifically to derive information on the cloud base height (see Figure X) and vertical visibility height. Cloud base height estimates for up to 3 layers, as well as the depth of penetration into low-level fogs, are derived operationally by the Vaisala software. Operations during leg #2 of the cruise have been continuous. Other than correcting the height measurements for the height of the ceilometer relative to the sea surface the raw measured data set will likely be the final data set. A single daily ASCII file is typically produced in standard Vaisala formats with naming convention CYMMDDhh.DAT, where Y is the last digit of the current year, MM is the month, DD is the day, hh is the hour. Total data volume for leg 2: 1 GB.

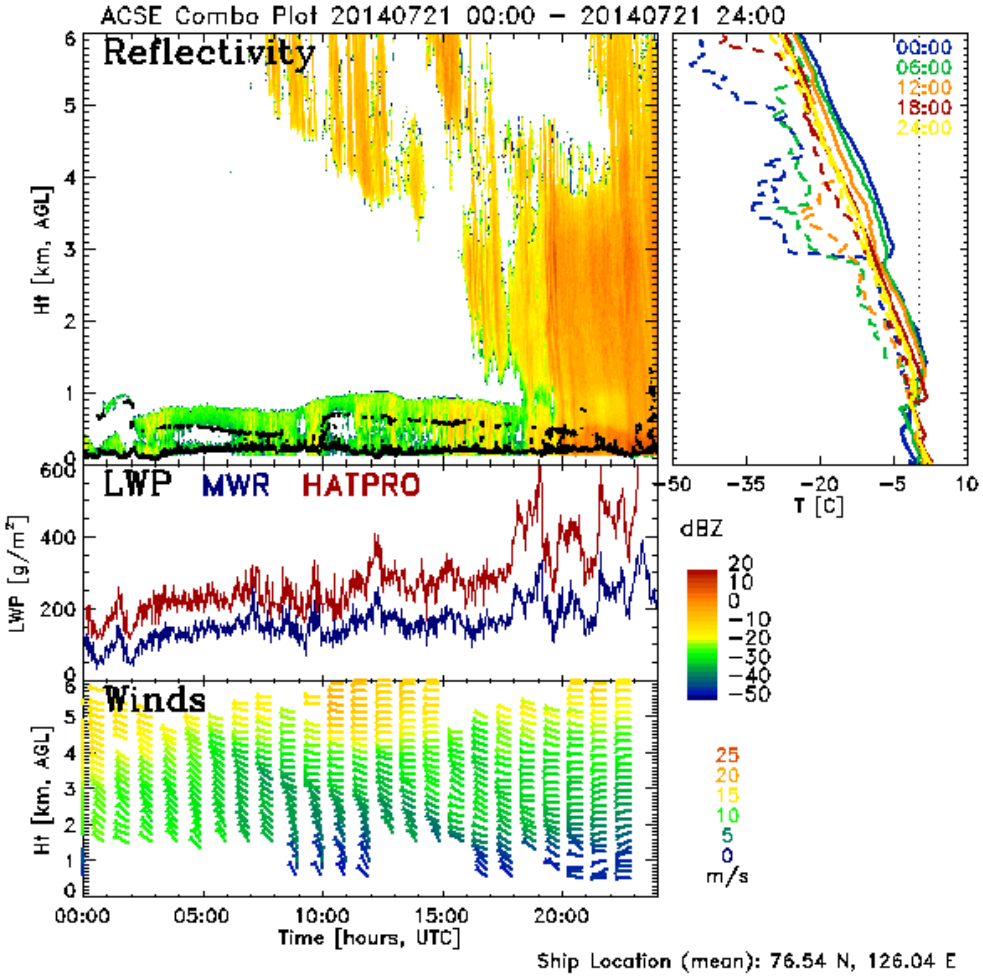

Figure BLM8. Example of results showing measurements on 21 July 2014, including time-height color contour of W-band radar reflectivity including ceilometer cloud base height (black dots) in top panel; derived cloud liquid water path from microwave radiometer and HATPRO in middle panel; derived profiles of wind speed and direction from the 449-MHz wind profiler in the bottom panel; and radiosonde temperature profiles in the panel to the right for context.

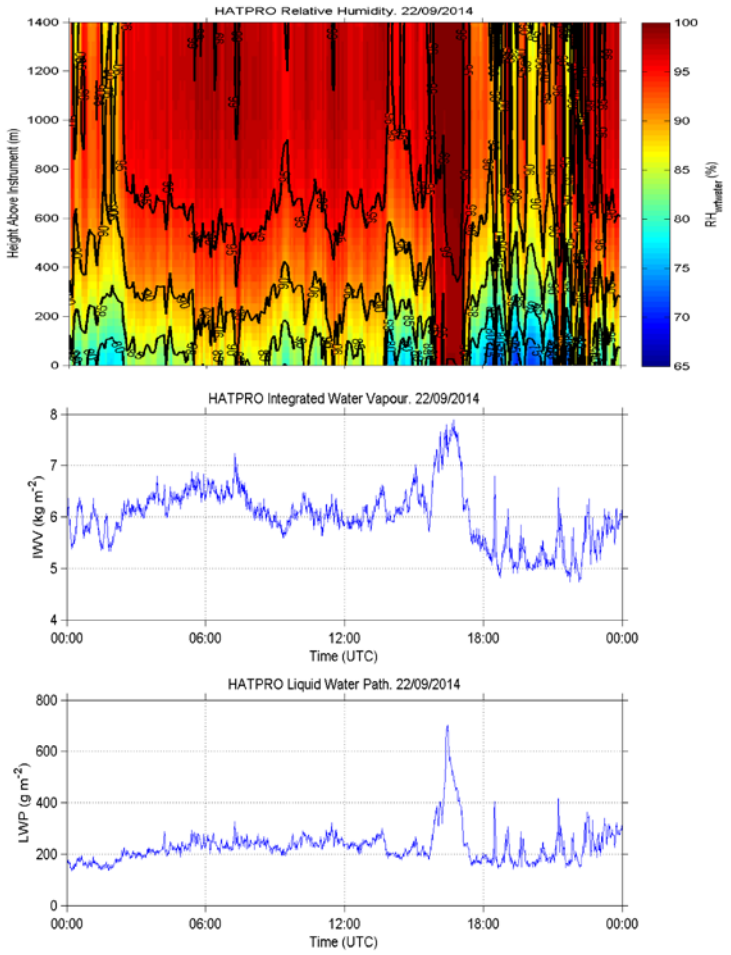

Fig. BLM9: Example of some of the data from the HATPRO scanning radiometer: Time-height cross-section of temperature to 1400 m height (top), vertically-integrated water vapor (middle), and liquid water path (bottom) as observed by the HATPRO radiometer for Sep. 22, 2014 (YD 265).

Miscellaneous observations

Some complementary observations were also made, in support of the main observations:

1. Surface skin temperature: Infrared surface temperature estimates were made with two Heitronics KT15.85 IR temperature sensors. Both are mounted on the starboard rail of the 7th deck (Fig. BLM3), one pointing about 45° forward and one 45° aft. Both are angled out to measure outside the ship wake in open water. Data is available immediately, however, a refined and quality controlled data set will be available within about 6 months. Data volume: 12MB per day (500 MB for Leg 2).
2. Surface imagery: Three webcams were installed on the rail on 7th deck (Fig BLM3), pointing forward, port and starboard. Each camera has a 90° field of view and records one image per minute. Imagery will be used to provide a visual record of the surface conditions through the cruise, and potentially estimates of local ice fraction. Data volume: approximately 250GB for Leg 2.
3. Surface waves: Datawell DWR-4-G Waverider buoy was deployed, tethered to the ship on a 200-m line. The waverider measures the 3-dimensional velocity of the buoy, integrating to obtain the displacements, from which directional wave spectra and basic wave statistics can be derived: significant wave height, wave periods (zero crossing, period of spectral peak, 'energy' period, etc.). For Leg 2, Waverider measurements were obtained on numerous occasions during coring and/or CTD stations outside the pack ice and in large open-water areas within the pack ice (Fig. BLM10). Twenty-two stations obtained wave data for 30-198 minutes (see Table 1). Over 38 hours of good data was obtained, with over 30 hours of those occurring during Leg 2. Local fetch information

associated with the buoy deployment is obtained from photographs of the ship's navigation X-band radar screen during pack-ice deployments. Three deployments were done in the Russian EEZ; one of these acquired no useful data because it did not drift away from the ship. (1 MB data for Leg 2)

Table 1: Times, locations and notes of the waverider buoy deployments during ACSE. Those done in the Russian EEZ are marked in red.

Number	Date	DoY	Lat	Lon	In	Undist.	Recovery	Good Dur.
			deg N	deg E	Water	Waves	Begins	min
1L1	7/18/2014	YD199	76.774	125.830	13:18	-	15:00	0
2L1	7/19/2014	YD200	76.893	127.798	12:50	13:00	18:29	329
3L1	8/14/2014	YD226	74.322	-171.444	22:25	22:27	23:50	83
4L1	8/15/2014	YD227	74.398	-169.671	3:24	3:26	4:30	64
1L2	8/26/2014	YD238	72.821	-175.486	6:30	-	-	0
2L2	8/28/2014	YD240	75.172	179.875	21:10	21:25	22:55	90
3L2	8/28/2014	YD240	75.143	179.862	22:50	22:52	23:30	38
4L2	8/29/2014	YD241	75.475	-179.757	20:27	20:34	21:55	81
5L2	8/30/2014	YD242	75.304	-179.627	6:50	7:00	7:45	45
6L2	8/30/2014	YD242	75.079	-179.988	21:38	21:52	23:54	122
7L2	8/31/2014	YD243	75.505	-179.092	7:58	8:05	8:40	35
8L2	8/31/2014	YD243	75.025	179.833	20:45	20:55	22:55	120
9L2	9/4/2014	YD247	76.4672	176.7894	1:00	1:10	2:00	50
10L2	9/4/2014	YD247	76.3642	176.4383	4:02	4:10	5:38	88
11L2	9/4/2014	YD247	76.3209	175.8902	8:02	8:13	9:27	74
12L2	9/6/2014	YD249	76.4074	173.9226	7:05	7:15	8:32	77
13L2	9/12/2014	YD255	79.8183	154.1786	3:22	3:25	3:56	31
14L2	9/12/2014	YD255	79.9228	154.3826	6:36	6:41	8:54	133
15L2	9/14/2014	YD257	81.3290	141.7355	3:20	3:25	5:40	121*
16L2	9/14/2014	YD257	81.0630	142.1099	9:00	9:03	10:05	62
17L2	9/14/2014	YD257	80.4743	142.9158	22:20	22:23	0:43	140
18L2	9/17/2014	YD260	80.7008	142.1143	6:35	6:39	8:11	92
19L2	9/20/2014	YD263	84.5113	151.9179	2:08	2:15	5:33	198
20L2	9/20/2014	YD263	85.1343	151.5701	21:33	23:01	0:43	102
21L2	9/22/2014	YD265	84.2690	148.7352	2:19	2:21	3:19	58
22L2	9/24/2014	YD267	84.7222	150.9535	22:45	22:55	0:07	72

Figure BLM10: Waverider buoy deployment on Sep. 17 and a close-up photograph of the buoy.

At-sea post-processing

Post-processing at sea of this data is limited to preliminary quality control analyses, producing quick-look images, and organizing/cataloging of the large amounts of data. Some preliminary correction for ship heading and speed over ground is done for the quicklook products involving wind data (e.g., the lidar and wind profiler; see Figs. BLM15 and BLM17). These same corrections and the corrections for the higher-frequency ship motion, such as heave, pitch, and roll, will be done in post-processing during the coming year for any data set measuring atmospheric motions, which include the lidar, turbulence, cloud radar, and wind profiler. Care is taken that all metadata is saved necessary to understand when, where, and under what conditions the various measurements were obtained, and that ancillary measurements necessary for post-processing corrections of the primary measurements is obtained. For example, measurements of the ship motion are made continuously that will be used to place the turbulence and remote sensor data into a fixed geophysical coordinate system rather than one moving with the ship. Other impacts on the data due to the shipboard nature of the measurements, such as shading of the radiometers by ship superstructure, must be estimated in order to correct the data. Because it is crucial to combine the various parameters measured during the analysis, care is also taken to carefully synchronize timestamps on the various data sets, generally to one second or better.

Also, processing on board has focused on comparing atmospheric structures as obtained by the different instrumentation systems to help guide later analyses. As an example, the radiometer relative humidity fields for a three day period as measured by the Radiometrics radiometer and the radiosondes are compared in Figure BLM11, showing that the radiometer tends to smooth and vertically elongate the vertical structures found in the radiosondes, and can be in error at higher altitudes. However, especially at lower altitudes, the radiometer is much better able to capture the temporal evolution of the humidity features, since these often have time scales of a few hours.

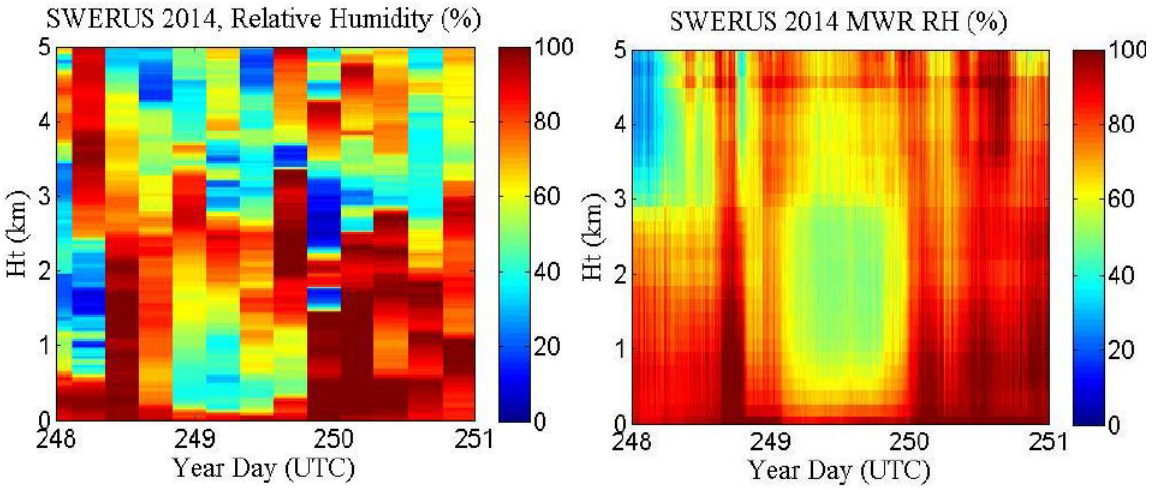

Fig. BLM11: Comparison of the relative humidity field from the surface to 5 km height for three days (Sep. 5-7) as observed by the 6-hourly rawinsondes (left) and the higher temporal resolution Radiometrics radiometer. Clearly, the vertical details that the radiosondes capture are greatly smoothed in the radiometer data, especially at upper levels, while the radiometer data provides better temporal resolution of the humidity features, which can often have time scales of a few hours or less.

Results – Metadata, data, and samples collected

WP BLM Boundary Layer Meteorology

The data collected will allow the analysis of the structure of the atmospheric boundary layer, clouds, and surface energy budget over the Arctic Ocean, including regions of open water, sea ice, and the marginal ice zone. The variety of measurements made will allow an improved understanding of the processes producing the complex interactions in these regions. Figure BLM12 shows an example of

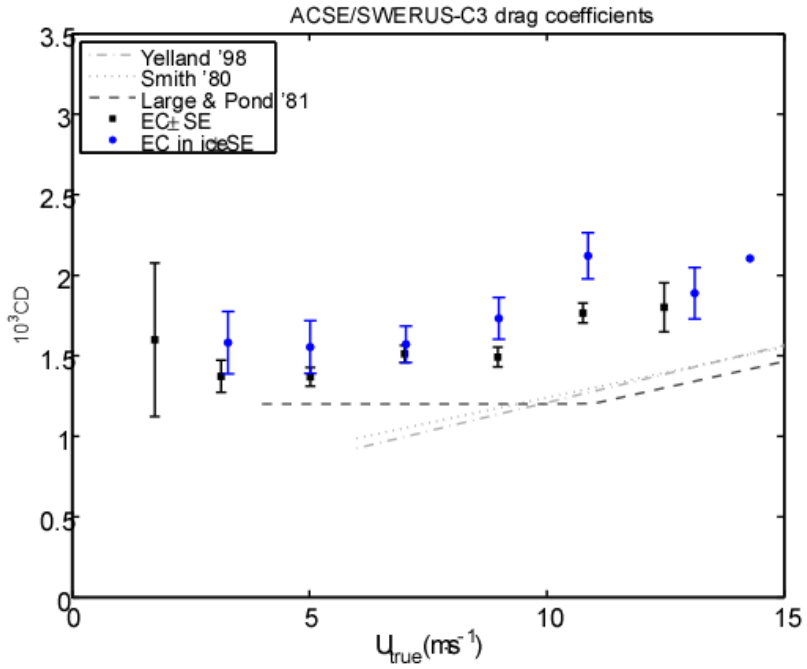

Fig. BLM12: Preliminary eddy covariance drag coefficient (CD) as a function of the wind speed as measured from the Metek sonic anemometer. Points are bin averaged, with error bars representing one standard deviation. Blue show those points from within the pack ice and black from open water outside the pack ice. The various dashed lines show relationships described by previous studies. The data has not been corrected for ship airflow distortion, though it has gone through basic quality control. The expected increase with wind speed is seen, as is the increase within the ice compared to open water.

preliminary results from the Metek sonic anemometer, where bin-averaged surface drag coefficients are plotted as a function of wind speed for within and outside the pack ice. The drag coefficient increases with wind speed as expected, while it is also larger within the pack ice compared to over open water. This is likely due to the large number of vertical roughness elements represented by the edges of the various ice floes when ice concentrations are near 40-60%, as suggested by Andreas et al (2010). In this case, the freezing-point surplus temperature of the 8-m water was used to define the in-ice/out-of-ice categories, rather than a sea-ice concentration.

Post-cruise analyses will also combine measurements from many of the sensors to provide a physical understanding of the active processes. As an example, Figures BLM13 through BLM17 show data from various instruments during the latter part of Leg 2 when the Oden was making measurements between 84 - 85 deg N within a large "bay" formed by the sea ice (see Fig. BLM2b). These data will provide detailed understanding of the likely complex interactions of synoptic scale, mesoscale, and microphysical atmospheric processes producing structures seen in these figures, and resulting in a surface energy budget producing the freeze-up of the Arctic Ocean in the vicinity of multi-year sea ice. The upper-level rawinsonde (Fig. BLM13) and windprofiler (Fig. BLM15) data reveal some of the large-scale synoptic evolution, while the lowest 500 m likely include changes from mesoscale interactions with the nearby ice edge. The vertical potential temperature gradient (Fig. BLM13a) shows predominantly near-neutral conditions in the lowest 400 m, consistent with the fairly turbulent conditions (Fig. BLM6c) with strong winds through the boundary layer (Fig. BLM17). The period of colder temperatures seen in the rawinsonde data occurred at the northern end of the "bay", while the coldest air in the lowest 500 m occurred when airflow came directly from the ice to over the Oden, as shown by the various wind measurements (Figs. BLM13b, BLM15, BLM17). A low-level jet (Fig. BLM15) occurs in the off-ice flow at the upper portions of this cold air (Fig. BLM13a) just below the clouds (Fig. BLM13b, BLM14), and likely represents a feature formed by the mesoscale thermal gradients in this region. The cloud radar (Fig. BLM14) and lidar data (Fig. BLM 16) show some of the macro and

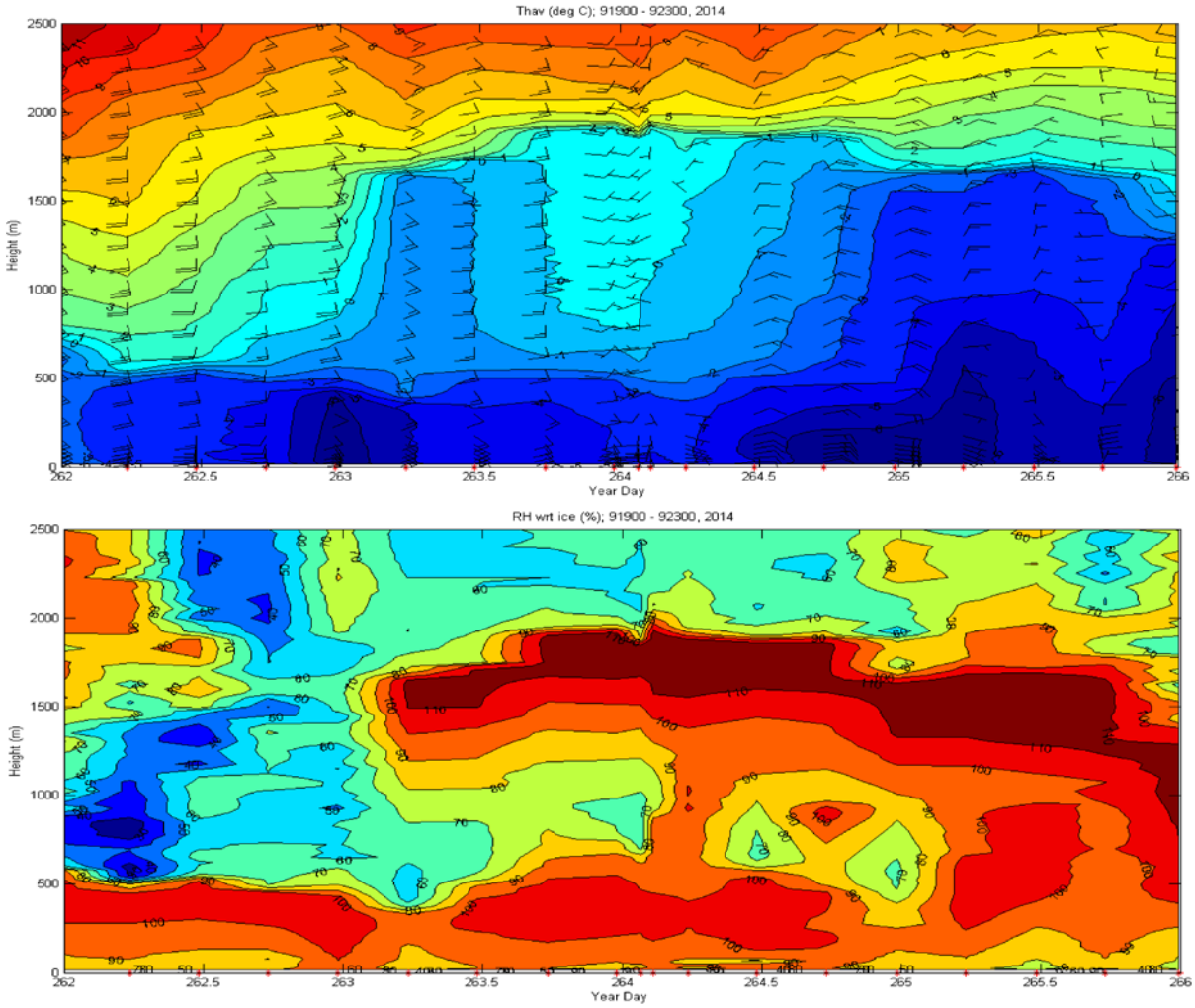

Fig. BLM13: Time-height cross-section of virtual potential temperature (deg C) and wind barbs (top) and relative humidity with respect to ice (%, bottom) in the lowest 2500 m from the rawinsondes launched from the R/V Oden during YD262-265 (Sep. 19-22, 2014).

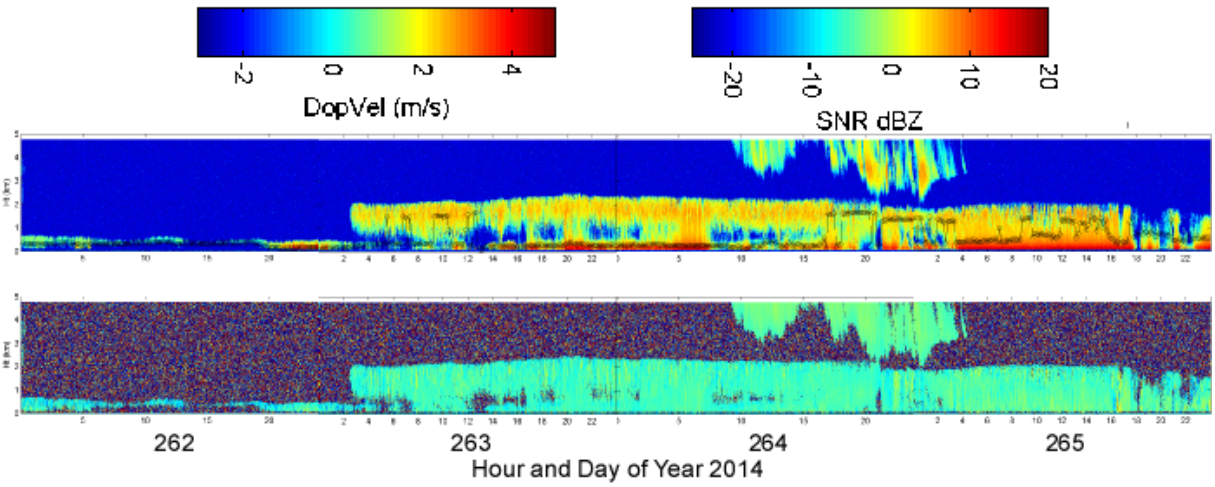

Fig. BLM14: W-band cloud radar signal-to-noise ratio and ceilometer cloud base height (open circles) (top) and W-band vertical velocity (bottom) for Sep. 19-22 (YD262-265). The lowest 5 km of the atmosphere is shown. The weak downward vertical velocities of < 1.5 m/s indicate snow or ice crystals.

microphysical aspects of these clouds that impacted the available solar and longwave radiation. The lidar data shows that the upper part of the low-level clouds was dominated by spherical particles, most likely supercooled liquid water, which strongly modulate radiative fluxes. Combined turbulent surface sensible and latent heat fluxes were positive (0 - +70 W m^{-2}), especially over the open water (Fig. BLM6c,d), contributing to the cooling of the ocean surface and the observed formation of sea ice. The radiation terms of the surface energy budget (not shown) are determined from measurements at the top of the 7th deck of the Oden (Fig. BLM3b), while changes to the ocean surface are documented by the surface temperature measurements and video imagery. The microwave radiometers provide additional temporal information on the boundary-layer heat and moisture evolution. The turbulence sensors also provide a direct measurement of the momentum flux (Fig. BLM6b), which are linked to the surface waves over the open ocean that may have had an impact on the observed ice formation, and waverider buoy deployments will show some of the wave spectra characteristics.

Clearly, the analyses to be done on this data set obtained during ACSE/SWERUS must combine the large variety of measurements and will require coordinated work in order to provide a clearer picture of the various processes involved in this complex physical system.

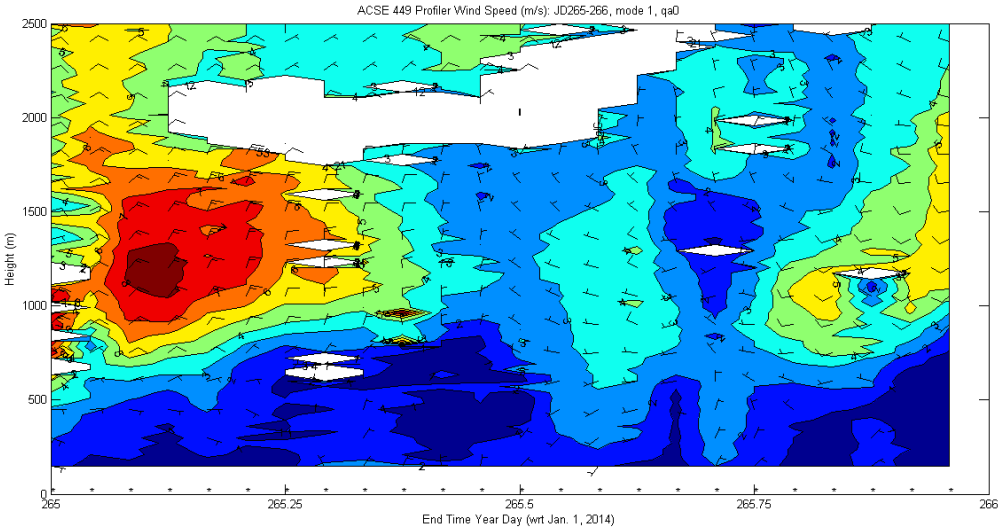

Fig. BLM15: Time-height section of isotachs and wind barbs derived from the 449 MHz wind profiler data for Sep. 19-22 (YD262-265). A low-level jet centered at about 1100 m is present in the off-ice NE winds on Sep.22

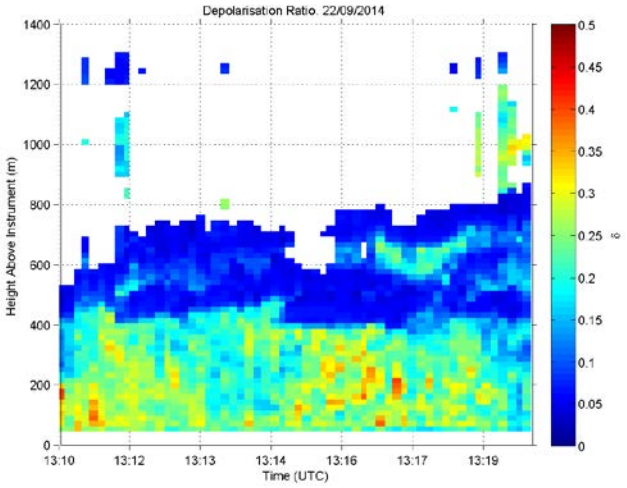

Fig. BLM16: Example of a time-height cross-section of the lidar depolarization ratio [ratio=B_cross/ (B_cross+B_parra)] near 13 UTC on Sep. 22 (YD 265). The low values indicate spherical particles, likely liquid drops at the tops of these lower clouds. The larger ratios below suggest the primary presence of ice crystals.

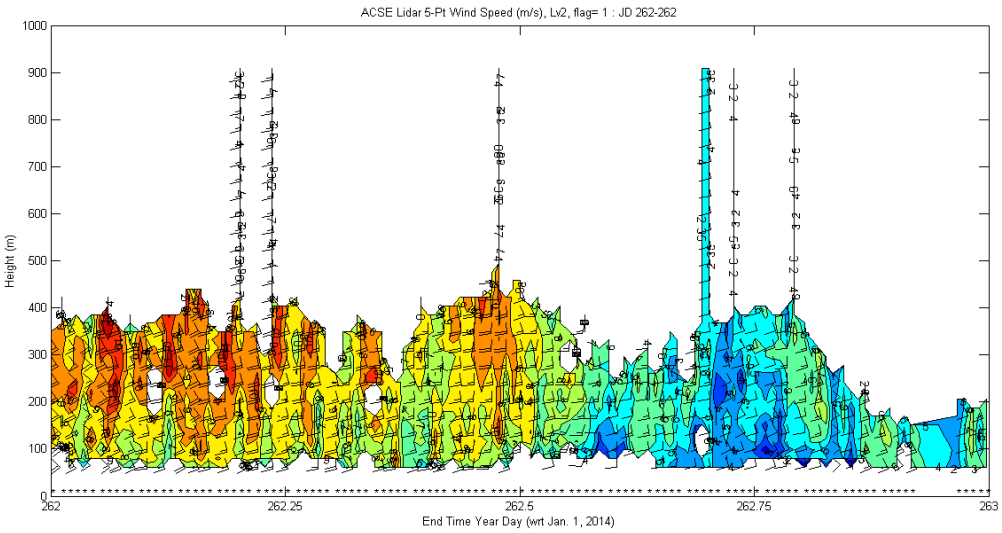

Fig. BLM17: Time-height cross-section of boundary-layer winds derived from the 5-beam lidar scan every 10 minutes during YD262 (Sep. 19). Shown are isotachs (m/s), with wind direction available from the wind barbs. Moderate 10 m/s SSE winds occur at the top of the boundary layer early in the day, which turned to due south by midday. The winds weakened later in the day, with some turning back towards the southeast. The stars at the bottom show the times when a good profile is encountered. This data is preliminary, as it has not been corrected for the ship's tilt at the exact time of each beam measurement.